https://doi.org/10.5194/acp-2019-565
Preprint. Discussion started: 15 July 2019

Atmospheric Chemistry and Physics Discussions

Variability of cirrus cloud properties using a Polly^{XT} Raman Lidar over high and tropical latitudes.

Kalliopi Artemis Voudouri[1], Elina Giannakaki[2,3], Mika Komppula[3], and Dimitris Balis[1]

[1]Laboratory of Atmospheric Physics, Physics Department, Aristotle University of Thessaloniki, Greece
[2]Department of Environmental Physics and Meteorology, Faculty of Physics, University of Athens, Greece
[3]Finnish Meteorological Institute, P.O.Box 1627, FI-70211, Kuopio, Finland

Correspondence: Kalliopi Artemis Voudouri (kavoudou@auth.gr)

Abstract. Measurements of cirrus clouds geometrical and optical properties, performed with a multi-wavelength Polly^{XT} Raman Lidar, during the period 2008 to 2016 are analysed. The measurements were performed with the same instrument, during sequential periods, in three places at different latitudes, Gual Pahari (28.43°N, 77.15°E, 243m a.s.l) in India, Elandsfontein (26.25°S, 29.43°E, 1745m a.s.l) in South Africa and Kuopio (62.74°N, 27.54°E, 190m a.s.l) in Finland. The lidar dataset has been processed by an automatic cirrus cloud detection algorithm. In the following, we present a statistical analysis of the lidar derived geometrical characteristics (cloud boundaries, geometrical thickness) and optical properties of cirrus clouds (cloud optical depth, lidar ratio, ice crystal depolarization ratio) measured in different latitudes that correspond to subtropical and subarctic regions as well as their seasonal variability. The effect of multiple-scattering from ice particles to the derived optical products is also considered and corrected in this study. Our results show that, over the subtropical stations, cirrus layers, which have a noticeable monthly variability, were observed between 7 to 13km, with mid-cloud temperatures ranging from -60°C to -21°C and a mean thickness of 1295 ± 489m and 1383 ± 735m for Gual Pahari and Elandsfontein respectively. The corresponding overall mean cirrus optical depth at 355nm is calculated to be 0.59 ± 0.39 and 0.40 ± 0.33, with lidar ratio values at 355nm of 26 ± 12 sr and 25 ± 6 sr, respectively. A more extended dataset was acquired for the subarctic area of Kuopio Finland, between 2012 and 2016. The estimated average geometrical thickness of the cirrus clouds over Kuopio is 1200 ± 585m and the temperature values vary from -71°C to -21°C, while the mean cirrus optical depth at 355nm is 0.25 ± 0.2, with an estimated mean lidar ratio of 33 ± 7 sr, similar to the lidar ratio values observed over middle latitude stations. The kind of information presented here can be rather useful in the cirrus parameterizations required as input to radiative transfer models, and can be a complementary tool to satellite products that cannot provide cloud vertical structure. In addition, a ground-based statistics of the cirrus properties could be useful in the validation and improvement of the corresponding derived products from satellite retrievals.

https://doi.org/10.5194/acp-2019-565
Preprint. Discussion started: 15 July 2019

Atmospheric Chemistry and Physics Discussions

1 Introduction

Cirrus clouds are formed in altitudes from 5 to 14km, having an average thickness of 1.5km and temperature variability from -80°C to -20°C. Cirrus are made predominantly, or entirely, of ice particles and the shape of their hydrometeors varies, affected by air temperature, atmospheric pressure, and ice supersaturation (Lynch et al., 2001). Given that cirrus clouds are challenging components in atmospheric and global climatological research, affecting the global radiation budget (e.g. Campbell et al., 2016), a number of studies have been focused on quantifying their geometrical, optical and microphysical properties (e.g. Seifert et al., 2007; Dionisi et al., 2013; Pandit et al., 2015). Furthermore, systematic monitoring and accurate characterization of cirrus properties are important in the evaluation of models and satellite retrievals and a detailed monitoring of their properties at different geographical locations is crucial to understand their effects on climate.

Active remote sensing techniques, such as lidar and cloud radar instruments, have proved to be useful tools in providing continuous monitoring of high spatial and temporal distributions of cirrus clouds boundaries and their properties, and thus, enhancing the opportunity of tracking cloud evolution both in time and in height. The capability of a cloud radar to map vertical and temporal structures of cloud layers has already been well recognized in the scientific community (Illingworth et al., 2007). Additionally, elastic backscatter and Raman lidars have also been used for retrieving geometrical and optical properties of cirrus clouds (i.e., Ansmann et al., 1992; Gouveia et al., 2017). Moreover, portable multiwavelength lidars (Polly^{XT}) allow for 24/7 monitoring of the atmospheric state (Engelmann et al., 2016) and can be used to establish long time series of aerosol or cloud measurements. Lidar observations also allow the retrieval of detailed hydrometeor properties, such as their sphericity, which is indicative of the shape of targets. The importance of ground-based lidar in monitoring cirrus clouds, is based on the mapping of particularly optically thin high altitude ice clouds which cannot produce sufficient reflectivity and as a consequence can be undetectable from cloud radars (Comstock et al., 2002) or from passive instruments. However, lidar beam attenuates effectively in liquid water clouds, and therefore, it is likely that in the case of multiple cloud layers reliable detection of cirrus clouds cannot be ensured.

In the last decades, efforts of observations of cirrus clouds properties have been conducted both in terms of field experiments (e.g. Seifert et al., 2007) and systematic observations (e.g. Dionisi et al., 2013; Pandit et al., 2015), in order to estimate their dependence on the geographical location. Dionisi et al. (2013) presented a methodology for identification and characterization of cirrus clouds properties, applied to the multiwavelength Rayleigh Mie–Raman (RMR) lidar in Rome. The study classified the detected cirrus clouds in different categories, based on their optical properties. Specifically, the analysis showed that 10% of the detected cirrus were subvisible clouds ($\tau < 0.03$), 49% thin ($0.03 < \tau < 0.3$) and 41% opaque cirrus ($\tau > 0.3$). The overall mean value of cirrus optical depth was calculated 0.37 ± 0.18, while the mean LR eff value was 31 ± 15 sr. Another statistical analysis on optical and geometrical properties of upper-tropospheric cirrus clouds based on a lidar dataset, was conducted in Amazonia (Gouveia et al., 2017). The frequency of occurrence of cirrus clouds classified as subvisible was 41.6%, whilst 37.8% was for thin cirrus and 20.5% for opaque cirrus. The correction of the multiple scattering effect to the optical products in this study was made following the model of Hogan (2008). Lakkis et al. (2015)revealed that the most commonly observed cirrus were characterized as optically thin cirrus, rather than opaque ones, with a mean optical depth value of 0.26 ± 0.11,

https://doi.org/10.5194/acp-2019-565
Preprint. Discussion started: 15 July 2019

Atmospheric Chemistry and Physics Discussions

over Buenos Aires (34.6°S, 58.5°W). Nevertheless, comparison on cirrus cloud properties performed with ground-based lidar systems for long periods at different geographical locations are scarce. However, observations that correspond to different areas and atmospheric conditions are crucial to reveal information of the aerosol effect on the geometrical and optical characteristics of the detected cirrus layers. That kind of observations can be further used in the validation of the satellite retrievals, which provide global distribution of cirrus clouds (Sassen et al., 2008).

The aim of this work is firstly to provide cirrus geometrical and optical properties in different hemispheres, based on ground-based lidar data and secondly to attribute any observable differences of cirrus properties to the subarctic and subtropical counterparts. The manuscript is structured as follows: after a brief description of the portable lidar system (Polly^{XT}) in Section 2, we present the data analysis algorithm in Section 3. Section 4 describes the methods applied for the optical products retrievals. A lidar derived statistical analysis and seasonal variations of geometrical and optical properties of cirrus clouds in both subtropical and subarctic areas over the period 2008–2016 is presented and discussed in Section 5. Concluding remarks are presented in Section 6.

2 Instrument and Measuring Sites

A multi-wavelength depolarization Raman lidar Polly^{XT} of the Finnish Meteorological Institute (FMI) performed automated measurements during the period 2008-2016 in three different geographical regions. The system is based on a compact, pulsed Nd:YAG laser, emitting at 355, 532 and 1064 nm, at 20 Hz repetition rate. The laser beam is pointed into the atmosphere at an off-zenith angle of 5°, so the impact of the specular reflection by ice crystals into cirrus layers on the backscattered signals is negligible. The backscattered signal is collected by a Newtonian telescope, with 0.9m focal length. The vertical resolution of the signal profiles is equal to 30m and the temporal resolution is 30s. The setup of the system includes two Raman channels at 387 and 607 nm, three elastic channels at 355, 532 and 1064 nm, a depolarization channel at 355nm (for India and South Africa), a water vapour channel at 407nm and depolarization channel at 532nm (cross- polarization with respect to the initial emitted polarization plane) for Kuopio. Detailed description of the system is provided in Althausen et al., 2009 and Engelmann et al., 2015. All measurements processed within the period 2008-2016 are available online at http://polly.tropos.de. A more detailed description of the system components is presented in Table 1. The Polly^{XT} has participated in two campaigns in two subtropical areas, within the framework of the EUCAARI (European Integrated project on Aerosol Cloud Climate and Air Quality interactions) project (Kulmala et al., 2011), covering a wide range of cloud types. Measurements have been performed in Gual Pahari (28.43°N, 77.15°E, 243m a.s.l) in India from March 2008 to March 2009 (Komppula et al., 2012), and in Elandsfontein (26.25°S, 29.43°E, 1745m a.s.l) about 150km from Johannesburg in South Africa from December 2009 to January 2011 (Giannakaki et al., 2015). The measurements in Elandsfontein were performed almost continuously, as two periods were dedicated to the maintenance of the system (the one from December 23 rd to January 26th 2009 and the second one, from October 23rd to November 23 rd 2010). Since November 2012 the Polly^{XT} is operating in Kuopio (62.74° N, 27.54°E, 190m a.s.l) in Finland providing continuous measurements and information for the presence of clouds of the subarctic area (Filioglou et al, 2017). The three measurement sites constitute regions with different atmospheric conditions and different

https://doi.org/10.5194/acp-2019-565
Preprint. Discussion started: 15 July 2019

Atmospheric Chemistry and Physics Discussions

nature and sources of aerosol. Evaluation of this cirrus dataset in various latitudinal experimental sites will provide valuable information of the regional characteristics of the measured cirrus properties.

3 Description of the cirrus retrieval algorithm

Several steps were followed for the processing of the range corrected signal at 1064nm derived by the Polly^{XT} , needed for the estimation of the cirrus boundaries. These are illustrated in Figure 1. First we applied an automatic algorithm to the raw signal of the Polly^{XT} for the detection of the cirrus clouds layers. The method used here is based on a Wavelet Covariance Transform (WCT) (Eq. 1), which detects discontinuities in the lidar signal, such as the top of the boundary layer, elevated aerosol layers or cloud boundaries, allowing the detection of cirrus cloud base and top (Brooks, 2003).

$$WCT = \sum_{b-\frac{\alpha}{2}}^{b} P(z)z^2dz - \sum_{b}^{b+\frac{\alpha}{2}} P(z)z^2dz \tag{1}$$

$$SNR = \frac{Csig}{\sqrt{Csig + Cbg}} \tag{2}$$

In Eq. 1, P(z) is the product profile where the WCT is being applied to. In our case, we apply the wavelet to the range corrected signal at 1064nm, after performing the following steps: a) the zero and background levels are subtracted, b) the signal is normalized with a maximum value below 1.5km, so as to enhance the applicability of the method in various atmospheric conditions and c) the signal to noise ratio (SNR, Eq. 2) (Georgousis et al., 2015) is above 3.5, since the lidar signal is strongly attenuated at higher altitude levels. It was found that above this threshold the WCT layer estimates were independent from SNR.

WCT is the result of the transformation, z is the altitude, β is the height at which a noticeable change in the normalized signal occurs, and α is the dilation chosen. A critical step to the accurate WCT application to the signal is the selection of an appropriate value of the window (dilation), so as to distinguish cloud layers from aerosol layers. In our case, a dilation of 225m, is chosen, proportional to the cirrus geometrical depth (Baars et al., 2008). Another critical step is the threshold WCT value for the determination of the cirrus boundary. A threshold value of 0.1 is selected as a detection limit for both the base (-0.1) and the top (+0.1) of cirrus cloud by Baars et al. (2008) after sensitivity studies.

The WCT transformation has already been applied successfully on cirrus cloud detection (Dionisi et al., 2013). The application of the WCT on a case of cirrus layer observed on July 20th 2016 at Kuopio station, for a time period between 01:00 and 05:00 UTC is presented. In our study, 60-min averages are computed and the respective mean value are taken as cloud base and top height. The mean wavelet applied to the corrected 1064 signal and the particle Depolarization ratio for the whole period of study of the cirrus evolution are presented in Fig. 2.

Finally, cloud retrievals from the algorithm are classified as cirrus clouds when the following three criteria were met: a) the particle linear depolarization value is higher than 0.25, b) the altitude is higher than 6km and c) the base temperature is below

https://doi.org/10.5194/acp-2019-565
Preprint. Discussion started: 15 July 2019

Atmospheric Chemistry and Physics Discussions

-20°C. The application of these criteria is made so as to avoid water clouds. It should be pointed out that lidar measurements were processed only in the absence of lower tropospheric (below 4 km) thick clouds.

4 Optical properties of cirrus clouds

4.0.1 Retrieval of the optical properties of cirrus

The integration of the extinction profile between the defined cloud base and the top of the cirrus layer is calculated to obtain the cirrus optical depth (COD) from the lidar measurements as shown in Eq. (3).

$$COD = \int_{z_{base}}^{z_{top}} a(z)dz \tag{3}$$

The night-time measurements from Polly^{XT} were processed by the Raman method, which allows the independent determination of the extinction and backscatter coefficients, thus providing the Lidar Ratio (extinction-to-backscatter ratio) (Ansmann et al., 1992). For the retrieval of the cirrus extinction coefficient profiles obtained from the daytime measurements, the integration of the backscatter profile multiplied by the lidar ratio is calculated. The daytime measurements from Polly^{XT} were processed using the Klett inversion (Klett, 1981; Fernald, 1984), with respect to the ratio of the extinction to the backscatter coefficient. These two unknowns have to be related using either empirical or theoretical methods in order to be able to invert the lidar equation. The lidar ratio was determined by comparing the forward and the backward solution of Klett. In our study, the effective lidar ratio was chosen when the aforementioned profiles tend to coincide (Ansmann et al., 1992). Both the daytime and night-time optical products were derived for each 1hour averaged profiles. The calculation of the corresponding molecular backscatter and extinction profiles was made based on temperature and pressure profiles obtained from radio soundings. Radiosondes launched daily at 06 and 18 UTC at the Jyvaskyla Airport, located to the southwest (62.39°N, 25.67°E) of the lidar station at Kuopio were used. Radiosonde observations released at Safdarjung Airport (28.58°N, 77.20°E) in New Delhi, India twice a day, and radiosondes from Upington International Airport (28.40°S, 21.25°E), in South Africa were used in the processing of the other two sites Another important lidar quantity is the particle depolarization ratio. This ratio constitutes a qualitative way to discriminate particle shapes and to distinguish spherical from non-spherical particles. Cirrus generally cause enhanced particle depolarization values, higher than 0.25 (see for e.g. Chen et al., 2002), depending on the ice-particle shape and orientation (Lynch et al., 2001). The calibration of the depolarization measurements was determined by using the geometric mean of the two $\pm 45°$ measurements, following the procedure described by Freudenthaler et al., (2009). The particle depolarization ratio is presented only for the dataset of Kuopio, as for the other two sites only the Rayleigh calibration method for the calibration measurements was available.

https://doi.org/10.5194/acp-2019-565
Preprint. Discussion started: 15 July 2019

Atmospheric Chemistry and Physics Discussions

4.0.2 Multiple scattering correction on optical products

The lidar equation assumes single scattering from the hydrometeor, but eventually the received photons could have been scattered multiple times before reaching the telescope. This effect, named multiple scattering, is considerably important primarily to the measured extinction coefficient values of cirrus clouds, and secondly to the calculated cirrus optical depth and the estimated Lidar Ratio values. Multiple scattering depends not only on cloud optical depth and cloud extinction, but also on the lidar system components, such as the laser divergence and the full-angle field-of-view of the receiver.

The relative influence of multiple scattering decreases with increasing height within the cloud, and the errors of the extinction coefficient can be even equal to 60% at the cirrus base (Lynch et al., 2001). Generally, multiple scattering effect cannot be negligible in a receiver field of view equal to 1mrad (Wandinger, 1998). Thus, this effect on cirrus clouds optical properties was considered and corrected in this study. In order to calculate the multiple scattering contribution to the calculated optical products, the Eloranta model (Eloranta, 1998) was used to estimate the ratio between the total received power and the contribution of the single scattering, the ratio $P_{tot}(z)/P_1(z)$ (Eq. 4).

The effective extinction coefficient aeff is then related to the actual (single scattering) coefficient a(z) through the parameter F as shown in Eq. (5) (Wandinger, 1998). This model assumes cirrus made up of hexagonal ice crystals. The estimation of the cirrus effective radii was taken from Wang and Sassen (2002), based on the linear relation of the effective radius with the cirrus cloud temperature derived from radio soundings. This model has already been validated against other models (Hogan, 2006) in order to correct the derived optical characteristics of cirrus clouds and has already been applied in cirrus lidar applications (for e.g. Giannakaki et al. 2007). In the following sections, the cirrus optical properties (lidar ratio, extinction coefficient, and optical depth) derived in the frame of this study were corrected for multiple scattering.

$$F(\lambda,z) = \frac{\frac{d}{dz} ln \frac{P_{tot}(z)}{P_1(z)}}{2a_{eff}(\lambda,z) + \frac{d}{dz} ln \frac{P_{tot}(z)}{P_1(z)}} \tag{4}$$

$$a_{par}(\lambda,z) = \frac{a^{eff}(\lambda,z)}{1 - F(\lambda,z)} \tag{5}$$

5 Results and discussion

In the following section, we present the mean geometrical and optical properties of the detected cirrus layers within the period 2008-2016 from the three measurement sites, which correspond to subtropical and subarctic regions, and we investigate the expected correlations between the retrieved properties.

5.0.1 Cirrus cloud cover detection

Cirrus cloud detection over the three regions is presented in Fig. 3. The analysis of measurements over Kuopio showed that the cirrus cloud cover was found to vary both diurnally and seasonally. From the available data, the frequency of cirrus clouds

https://doi.org/10.5194/acp-2019-565
Preprint. Discussion started: 15 July 2019

Atmospheric Chemistry and Physics Discussions

appears to exhibit an annual pattern with the maximum occurrence from April to October and minimum occurrence during the period between November and January, given the favorable meteorological conditions, with no lower clouds. Layers of low-water clouds were present all year long, with the peak of monthly occurrence between April (28 cases) and November (27 cases). This monthly pattern follows the annual temperature cycle over the region (Jylhä, et al., 2004), with maximum temperature values observed during the period April to October, while November to February are the coldest months. Concerning the diurnal pattern, the frequency of cirrus clouds during night-time is higher from February to July, and smaller in the period from August to January.

A similar annual pattern of cirrus occurrence frequencies is found over Elandsfontein, but with maximum occurrence during May and December. No data processing could be performed during unfavourable weather conditions, such as the presence of low cloud, observed mainly the months between January to April with a percentage of $\sim 30\%$ of the measurement period.

Temperature time series over the region shows that the cirrus occurrence follows the temperature seasonal cycle, with the minimum values during June-July and the maximum during December (Laakso, et al., 2012). The limited dataset over Gual Pahari (given the periods with technical issues) cannot provide any monthly trend and cannot be representative of the cirrus cloud occurrence. Also, the occurrence rate of low clouds between March and Septembre, minimize the dataset.

5.0.2 Optical and geometrical properties of cirrus clouds over the sub-arctic station of Kuopio (62.74°N, 27.54°E, 190m a.s.l)

Mean cirrus cloud thickness reported in literature is about 2.0 km globally (Sassen et al., 2008), while lower thickness values from ground-based systems have been reported (e.g., Gouveia et al., 2017). In this study the mean geometrical thickness is calculated to be 1200 ± 585m. Seasonal mean cirrus cloud-base heights are calculated as follows: 8725 ± 1169m (MAM), 8542 ± 1120m (JJA), 8594 ± 1100m (SON), and 8300 ± 1390m (DJF) with an annual mean value of 8597 ± 1080m. The vertical distribution of cloud-base heights shows a broad monthly distribution ranging from 6440m to 11980m. The variability in monthly cirrus cloud base and top heights is shown in Fig. 4. The annual mean of the upper boundary of cirrus layers is 9480 ± 1075m, with a maximum value of 12490m during August. Base cirrus temperatures range from -63°C to -23°C having a mean value of -40°C. The corresponding temperature values of the top, range from -71°C to -31°C, with a mean value of -48°C. These values are in accordance with the corresponding ones from the combined data of CloudSat and CALIPSO (Cloud-Aerosol Lidar and Infrared Pathfinder Satellite Observations) measurements (Sassen et al., 2008).

In this study, the extinction coefficient at 355nm, averaged over every 1 hour of measurements, ranged from 1.879e-06 to 2.7e-04, with an annual mean value of 5.47e-05 ± 4.3e-05m -1 . Seasonal mean extinction values were calculated as: 5.47e-05 ± 4.4e-05 (MAM), 5.22e-05 ± 3.6e-05 (JJA), 5.24e-05 ± 3.5e-05 (SON), and 7.975e-05 ± 7.2e-05 (DJF). The corresponding values for the backscatter coefficient range from 1.51e-07 to 9.96e-06 with an annual value of 1.769e-06.

Column-integrated mean corrected COD at 355nm is 0.25 ± 0.2, and is found to vary between 0.018 and 1.53, while the mean COD 532 is found to be 0.231 ± 0.18. The highest values of AOD are found between January and March. To further investigate the distribution of the cirrus optical depth, we present a histogram of cirrus cloud optical depth in Fig. 5a and Fig. 5b. The most predominant values of cirrus optical depth are between 0.1 and 0.4. The mean COD 355 calculated in this study

https://doi.org/10.5194/acp-2019-565
Preprint. Discussion started: 15 July 2019

Atmospheric Chemistry and Physics Discussions

is larger than the value of 0.16 ± 0.27 reported by Das et al. (2009) and smaller than the value of 0.41 ± 0.68 reported by Min et al. (2011) from mid-latitude observations. And at the same time, a number of studies reported mean COD values between 0.2 and 0.4. The mean cirrus optical depth reported for a tropical region is 0.25 ± 0.46 (Gouveia et al., 2017), while the overall mean value of cirrus optical depth for a midlatitude station found to be 0.37 ± 0.18 (Dionisi et al., 2013). Reichardt (1998) reported that cirrus clouds optical depth values were lower than 0.3 for 70% of the cases processed for northern midlatitude cirrus. The classification of cirrus clouds according to Sassen and Cho (1992) indicates that 3.1% of the cirrus clouds measured in Kuopio are subvisible ($\tau < 0.03$), 70% are thin cirrus ($0.03 < \tau < 0.3$) and 26.9% are opaque cirrus ($\tau > 0.3$). The low percentage of the subvisible category of cirrus layers, have also been observed over midlatitude sites (e.g., Kienast-Sjögren et al., 2016), where subvisible cirrus clouds have been measured during 6% of the observation time.

A mean value Lidar Ratio of 33 ± 7 sr at 355nm is observed for the whole period studied, with a variability of less than 1.5 sr for the different seasons (Fig. 6), while the corresponding mean value LR 532 is calculated to be 30.4 ± 7.5 sr, without any obvious seasonal cycle. Specifically, the mean LR 355 for the corresponding months are calculated as follows: 33 ± 7 sr (MAA), 33.2 ± 7.3 (JJA), 32.9 ± 7 (SON) and 32.3 ± 5 (DJF). For opaque, thin and sub-visible cirrus clouds the means are 30 ± 6 sr, 33.8 ± 7.1 sr, and 34.4 ± 7.4 sr, respectively. Gouveia et al. (2017) found a mean LR 355 value of 23.9 ± 8.0sr (SD) for the tropical region of Amazonia, while Giannakaki et al., (2007), reported a corresponding value of 30 ± 17sr for a mid-latitude station. Josset et al. (2012) and Garnier et al. (2015) analyzed spaceborne CALIOP (Cloud Aerosol Lidar with Orthogonal Polarization) lidar observations. Both studies concluded that cirrus lidar ratio (corrected for multiple scattering effects) around the globe has typically values of 30–35sr ± 5–8sr at 532 nm. Nevertheless, the lidar ratio values may vary greatly depending not only on the altitude and composition of the cirrus clouds (Goldfarb et al., 2001), but also on the correction of the multiple scattering effect (Platt, 1981; Hogan, 2008). The aforementioned depends on the ice crystals effective radius and the associated uncertainty could range from 20 to 60% (Wandinger, 1998). Lidar ratio for cirrus clouds is assumed to be constant with altitude and season with a value of 25 sr using the CALIOP extinction retrieval algorithm (Young et al., 2013; Young and Vaughan, 2009). Fig. 5c and Fig. 5d presents the histograms of the lidar ratio corrected for multiple-scattering, with the most frequent observed lidar ratio values ranging between 28 and 36 sr for 355 nm and 20 and 36 sr for 532 nm. Similar results have been retrieved regarding the variability of LR 532 , which is constant from one month to another (not shown here).

In Figure 7, we examine the dependence of the LR 355 with the COD 355 values on intervals of 5 sr. The dashed lines indicate the categories defined by Sassen and Cho (1992). The most common lidar ratio values from 25 to 40 sr are found for the lowest COD values. Furthermore, the dependence of the lidar ratios at 355nm with the cirrus cloud base temperature is also examined. No dependence of the lidar ratio with cloud base temperature is found, indicating that cirrus are vertically well mixed (Liu et al., 2015).

5.0.3 Optical and geometrical properties of cirrus clouds over the sub-tropical region of Gual Pahari (28.43°N, 77.15 °E, 243m a.s.l) – Northern hemisphere

The cirrus lidar dataset in this region is the less extensive one compared to the other two sites and limitations due to the low signal to noise ratios exist. Indeed the sampling might not be statistically representative of the cirrus cloud properties, but some

https://doi.org/10.5194/acp-2019-565
Preprint. Discussion started: 15 July 2019

Atmospheric Chemistry and Physics Discussions

first results can be discussed. Specifically, during the one-year-long measurement period, Polly^{XT} was measuring on 183 days, corresponding to 2500h in total. The mean value of cirrus base is calculated 8947 ± 1465m, whilst mean top is found to be 10235 ± 1500m, with mean geometrical thickness of 1295 ± 489m. The temperature varied from -20°C to -50°C. The mean COD 355 is 0.59 ± 0.39 and the mean COD 532 is found to be 0.43 ± 0.37. The Lidar Ratio value at 355nm is calculated at 25.6 ± 12 sr and the corresponding one for 532nm is 27 ± 16 sr. The AOD have their highest values between May and August and the lidar ratios reach their highest values in May. The cirrus layers detected are mostly classified as opaque layers (68%).

Our results agree with another cirrus cloud study for the area; He et al. (2012) report a mean lidar ratio value of 28 sr, using a micropulse lidar. According to their study, the optical depth of the cirrus layers varied between 0.0004 and 2.6, with mean value of 0.33. The detected cirrus clouds were classified as follows: sub-visible cirrus (0%), optical thin cirrus (27%) and opaque cirrus (72%). One possible reason for the occurrence frequency of subvisible cirrus clouds in this dataset can be the lower SNR that does not allow detectability of optically thin clouds at Gual Pahari. Another study over North China (Min et al., 2011), based on CALIOP satellite measurements, reported a value of 1600 ± 1015m for the cirrus geometrical thickness. According to their study, the cirrus top temperatures were found lower than -50°C and higher than -80°C. Concerning the optical properties, a mean value of optical depth of 0.41 ± 0.68 at 532nm was reported. The detected cirrus layers were classified as follows: subvisible cirrus (30.26%), optical thin (34.59%) and opaque cirrus (21.54%).

5.0.4 Optical and geometrical properties of cirrus clouds over the sub-tropical region of Elandsfontein (26.25°S, 29.43°E, 1745m a.s.l) – Southern Hemisphere

A total measurement time of about 4935h corresponding to 88 cirrus profiles have been obtained over Elandsfontein, during the observation period between 11 December 2009 and 31 January 2011, with the exception of the two periods of maintenance of the system (mentioned above). From the cirrus profiles processed, the mean value of cirrus base is calculated to be 8477 ± 858m, while mean top at 10015 ± 906m for the region of South Africa and the mean geometrical thickness is 1383 ± 735m. The mean value of COD 355 is calculated at 0.4 ± 0.3 and the mean COD 532 is found to be 0.324 ± 0.319. The AOD have their highest values in the autumn and the lidar ratios reach their highest values in the autumn and winter. A percentage of 4% is categorized as subvisible cirrus, 52% as thin cirrus and 44% as opaque cirrus. The mean LR 355 value is found to be 25 ± 6 sr and the mean LR 532 is 24 ± 6 sr. As a limited number of long-term cirrus measurements are carried out in the Southern Hemisphere and only information from satellite observations have been published, especially for the geometrical properties (Sassen et al., 2008), no comparison with previous studies can be conducted for the region and the information reported here, to our knowledge, represents the longest ground-based lidar dataset of cirrus properties.

5.0.5 Cirrus classification

The classification of cirrus clouds according to Sassen and Cho (1992) is made based on the COD values. Ground-based lidars are well suited for thin cirrus layers observations, due to their sensitivity to thin atmospheric features, in contrast to spaceborne lidar observations (Martins et., 2011). For this reason, additional analysis on each cirrus category is also Conducted for Kuopio as measurements in this station represent the most extensive dataset with a set of 224 cirrus cases acquired between November

https://doi.org/10.5194/acp-2019-565
Preprint. Discussion started: 15 July 2019


Atmospheric Chemistry and Physics Discussions

2012 and December 2016.

275

Category "Subvisible"

Subvisible cirrus are geometrical thin layers with mean geometrical thickness of 643 ± 211 m. Generally, subvisible cirrus detection is a challenging component in satellite retrievals. MODIS, for example, is not sensitive to optically thin cirrus clouds due to the insufficient contrast with the surface radiance (Ackerman et al., 2008; Ackerman et al., 2010), while the CALIPSO
280 and CloudSat observations are more sensitive to the height and presence of subvisible and thin cirrus (Hong et al., 2010). Thus, the mapping of subvisible cirrus can be rather important in climatological studies. In our study, 6 cases of cirrus with COD less than 0.03 are analyzed, mostly detected during February. Subvisible cirrus geometrical thickness found 750 ± 269 m, less than the mean value of all cirrus clouds, and their temperature 2°C-3°C colder than the mean temperature. These values are consistent with previous studies of subvisible cirrus from spaceborne lidar observations, examined on a global scale (Martins
285 et., 2011). Their mean COD 355 is calculated 0.021 ± 0.0031, their mean LR 355 was 34 ± 7sr and their mean particle depolarization value is 0.45.

Category "Thin"

As mentioned previously, thin cirrus is the most predominant type of cirrus in our study, with 161 observations. Thin cirrus
290 can also be undetectable by passive remote-sensing satellites, especially the ones with COD less than 0.2, and have so far not systematically been characterized. Their geometrical thickness found to be 1100 ± 586 m. Their mean COD 355 is calculated 0.16 ± 0.07, their mean LR 355 is 34 ± 7 sr and their mean particle depolarization value is 0.3 ± 0.13.

Category "Opaque"

295 Opaque cirrus are the one with the highest value of optical depth that contribute the most of the total radiative forcing (Kienast-Sjögren et al., 2016). In our study, a total of 62 measurements of opaque cirrus are processed. Their mean geometrical thickness is found to be 1462 ± 659 m, higher than the value of all cirrus categories. Their mean COD 355 is calculated 0.5 ± 0.21, their mean LR 355 was 31 ± 6 sr and their mean particle depolarization value is 0.33 ± 0.12.

5.0.6 Temperature and latitudinal dependence of cirrus properties

300 The three datasets are derived from different latitudinal and climatic sites. In this section we examine the lidar products profile shape and the dependence of the geometrical and optical properties on cirrus base temperature. The mean and standard deviation of the Lidar Ratio and percentages of each cirrus class are listed in Table 2. Generally, cirrus layers have been observed up to altitudes of 13km above Gual Pahari, whereas they have only been detected to about 1km lower at the other two regions and this conclusion is in accordance with the Cloudsat observations (Sassen et al., 2008). Based on the satellite information,
305 the derived cirrus cloud thicknesses were found to be larger in the tropics and decreasing toward the poles. Also, larger values of COD 355 and smaller LR were observed for Gual Pahari and Elandsfontein. The larger variability of the optical properties at the two subtropical regions, relative to Kuopio, could be related to the larger and variable aerosol load over these regions.

https://doi.org/10.5194/acp-2019-565
Preprint. Discussion started: 15 July 2019


Atmospheric Chemistry and Physics Discussions

Overall, our results seem to demonstrate that subarctic cirrus clouds are colder, lower and optical thinner than subtropical cirrus clouds. However, a more extended database is needed to strengthen these indications.

The dependence of geometrical and optical properties on cirrus base temperature is also examined in Fig. 8. The number of cases per temperature bin are also labeled. In order to investigate this dependence, we have grouped cirrus clouds temperatures into 5°C intervals. Temperature values are obtained from radio soundings, as mentioned above. Thicker clouds ($\sim$ 1.5 km) are observed at temperatures $\sim$ -40°C, decreasing in thickness for lower temperatures, for both the subtropic and subarctic regions. This trend is also reported for a midlatitude region by Hoareau et al. (2013), where thickest cirrus layers were found about -42.5°C, and thinner ones at both colder and warmer temperatures. Concerning the optical properties shown in Fig. 10, there are indications that the cloud optical depth increases with the increasing cirrus temperature base for the two subtropical sites (Fig. 10c). At cold temperatures (-65°C), optical thickness for cirrus layers of the subarctic station is high, compared to warmer temperatures and also cloud thickness for this temperature is similar high ($\sim$ 1.5 km). The dependence of the lidar ratio and the particle depolarization values on base temperature is also examined (Fig. 10b and Fig. 10d). No clear tendency is found for the lidar ratio, as the variability of this parameter is relatively constant across months for both subarctic and subtropic regions, while the particle depolarization increases with the decreasing temperature base. This behaviour indicates a relation between cirrus ice crystal shape and temperature and has been also reported for a midlatitude station (Sassen et al., 2001). However, more studies should be done in order to examine this behaviour on various geographical locations.

6 Conclusions

Observations of cirrus clouds geometrical and optical properties, performed with a ground-based multi-wavelength Polly^{XT} Raman Lidar, during the period 2008 to 2016 are analyzed and presented in this study. The measurements were performed in three places at different latitudes, Gual Pahari (28.43°N, 77.15°E, 243m a.s.l) in India, Elandsfontein (26.25°S, 29.43°E, 1745m a.s.l) in South Africa and Kuopio (62.74 °N, 27.54°E, 190m a.s.l) in Finland. An algorithm is developed to automatically define the cirrus clouds boundaries. The vertical profiles of the backscatter, extinction, and lidar ratio and the monthly patterns of the geometrical characteristics and optical properties of cirrus layers are presented.

Our results show that cirrus layers having a noticeable month-to-month variation, with slightly higher geometrical values in summer compared to other seasons for the subtropical northern hemisphere. The statistical behaviour of the cirrus clouds properties in the different geographical and climatic counterparts shows that the geometrical boundaries display large distribution for the two subtropical regions with higher values of geometrical thickness, with mean thickness of 1295 $\pm$ 489m, 1383 $\pm$ 735m and 1200 $\pm$ 585m for Gual Pahari, Elandsfontein and Kuopio respectively, showing their dependence on the geographical location. The corresponding overall mean value of COD 355 is calculated to be 0.59 $\pm$ 0.39 and 0.40 $\pm$ 0.33, for Gual Pahari and Elandsfontein correspondingly, while a slightly lower mean of 0.25 $\pm$ 0.2 is calculated for Kuopio. The lidar ratio values at 355nm are found to be 26 $\pm$ 12 sr, 25 $\pm$ 6 sr, and 33 $\pm$ 7 sr for Gual Pahari, Elandsfontein and Kuopio, respectively. Generally the optical properties have their highest values in the subtropical region of the northern hemisphere. Overall, our

https://doi.org/10.5194/acp-2019-565
Preprint. Discussion started: 15 July 2019

results seem to demonstrate that subarctic cirrus clouds are colder, lower and optical thinner than subtropical cirrus clouds. However, a more extended database is needed to strengthen these indications.

The dependence of cirrus clouds geometrical thickness and optical properties on base temperature is also examined, showing quite similar tendency, but less variability for the subarctic dataset. Cirrus found geometrical thickest (geometrically and optically) at temperatures -40°C. At temperatures of -65°C, the optical thickness of cirrus layers is high, compared to warmer temperatures and also cloud thickness for this temperature is similar high ($\sim$ 1.5 km) and this trend appears only for the subarctic station. The lidar tatio is found to be quite constant with temperature, showing larger variability for the subtropic datasets, while the particle depolarization values increases with the decreasing temperature base.

The geometrical and optical properties of cirrus layers are studied in detail, providing information useful in the validation of the cirrus parameterizations in models. Furthermore, our results could be useful for lidar ratio selection schemes needed by satellite optical properties retrievals of cirrus layers over different locations, e.g., the upcoming EarthCARE (Earth Cloud Aerosol and Radiation Explorer) mission. In any case, further cirrus observations must be conducted, so as to investigate-whether differences in the background aerosol load contribute to potential differences in the cirrus cloud geometrical and optical properties.

Author contributions. KA. Voudouri prepared the automatic algorithm for the cirrus detection and processed the lidar measurments for the optical retrievals during the period 2008–2016. KA. Voudouri prepared the figures of the manuscript. E. Giannakaki reviewed parts of the results. M.Kompulla is the PI of the lidar station and D. Balis directed the preparation of the manuscript. KA. Voudouri prepared the manuscript with contributions from all co-authors.

Competing interests. The authors declare that they have no conflict of interest.

Acknowledgements. This work has been conducted in the framework of EARLINET (EVR1 CT1999-40003), EARLINET ASOS (RICA-025991), ACTRIS, and ACTRIS-2 funded by the European Commission. The research leading to these results has received funding from the European Union's Horizon 2020 research and innovation program under grant agreement no. 654109 and previously from the European Union Seventh Framework Programme (FP7/2007–2013) under grant agreement no. 262254. This work was partly funded by the European Commission 6th Framework under the European Integrated Project on Aerosol Cloud Climate and Air Quality Interactions, EUCAARI. Voudouri K.A acknowledges the support of the General Secretariat for Research and Technology (GSRT) and Hellenic Foundation for Research and Innovation (HFRI). (Scholarship Code: 95041).

https://doi.org/10.5194/acp-2019-565
Preprint. Discussion started: 15 July 2019

Atmospheric Chemistry and Physics Discussions

References

Ackerman, S., Holz, R., Frey, R., and Eloranta, E.: Cloud Detection with MODIS: Part II Validation, J. Atmos. Ocean. Tech., 25, 1073–1086, doi:10.1175/2007JTECHA1053.1, 2008.

Ackerman, S., Frey, R., Strabala, K., Liu, Y., Gumley, L., Baum, B., and Menzel, P.: Discriminating Clear-Sky From Cloud With MODIS, Algorithm Theoretical Basis Document (MOD35), ATBD Version 6.1, 2010.

Althausen D., Engelmann R., Baars H., Heese B., Ansmann A., Muller D., Komppula M.: Portable Raman lidar Polly^{XT} for automated profiling of aerosol backscatter, extinction, and depolarization. J.Atmos Ocean Tech 26:2366-2378. Doi10.1175/2009JTECHA1304.1, 2009.

Ansmann, A., Wandinger, U., Riebesell, M., Weitkamp, C., and Michaelis, W.: Independent measurement of extinction and backscatter profiles in cirrus clouds by using a combined Raman elastic-backscatter lidar, Appl. Opt., 31, 7113–7131, 1992.

Baars, H., Ansmann, A., Engelmann, R., and Althausen, D.: Continuous monitoring of the boundary-layer top with lidar, Atmos. Chem. Phys., 8, 7281-7296, https://doi.org/10.5194/acp-8-7281-2008, 2008.

Beyerle G., Gross M. R., Haner D. A., Kjome N. T., McDermid I. S., McGee T. J., Rosen J. M.,Schafer H. J., and Schrems O., "A lidar and backscatter sonde measurement campaign at Table Mountain during February–March 1997: observations of cirrus clouds," J. Atmos. Sci. 58, 1275–1287, 2001.

Brooks, I.: Finding Boundary Layer Top: Application of a wavelet covariance transform to lidar backscatter profiles, J. Atmos. Ocean. Tech., 20, 1092–1105, 2003.

Campbell, J., Lolli, S., Lewis, J., Gu, Y., and Welton, E.: Daytime Cirrus Cloud Top-of-the-Atmosphere Radiative Forcing Properties at a Midlatitude Site and Their Global Consequences, J., Appl. Meteorol. Clim., 55, 1667–1679, doi:10.1175/JAMC-D-15-0217.1, 2016.

Chen, Wei-Nai & Chiang, Chih-Wei & Nee, Jan.: Lidar Ratio and Depolarization Ratio for Cirrus Clouds. Applied optics. 41. 6470-6. 10.1364/AO.41.006470, 2002.

Comstock, J. M., Ackerman, T. P., and Mace, G. G.: Ground-based lidar and radar remote sensing of tropical cirrus clouds at Nauru Island: Cloud Statistics and radiative impacts, J. Geophys. Res., 107, 4714, doi:10.1029/2002JD002203, 2002.

Das, S.K., Nee, J.B., Chiang, C.W.: A LiDAR study of the effective size of cirrus ice crystals over Chung-Li, Taiwan. J. Atmos. Terr. Phys. 72 (9–10), 781–788. http://dx.doi.org/10.1016/j.jastp.2010.03.024, 2010.

Dionisi D., Keckhut P., Liberti G. L., Cardillo F., and Congeduti F.: Midlatitude cirrus classification at Rome Tor Vergata through a multichannel Raman–Mie–Rayleigh lidar, Atmos. Chem. Phys., 13, 11853–11868, www.atmos-chem- phys.net/13/11853/2013/doi:10.5194/acp-13-11853-2013 , 2013.

Eloranta, E.: Practical model for the calculation of multiply scattered lidar returns, Appl. Opt., 37, 2464–2472, doi:10.1364/ao.37.002464, 1998.

Engelmann, R., Kanitz, T., Baars, H., Heese, B., Althausen, D., Skupin, A., Wandinger, U., Komppula, M., Stachlewska, I.S., Amiridis, V., Marinou, E., Mattis, I., Linné, H., and Ansmann, A.: The automated multiwavelength Raman polarization and water-vapor lidar Polly^{XT} : the neXT generation, Atmos. Meas. Tech., 9, 1767-1784, https://doi.org/10.5194/amt-9-1767- 2016, 2016.

Engelmann R., Kanitz T., Baars H., Heese B., Althausen D., Skupin A., Wandinger U., Komppula M., Stachlewska IS, Amiridis V., Marinou E., Mattis I., Linne H., Ansmann A.: EARLINET Raman lidar Polly^{XT}: the next generation. Atmos Meas Tech Discuss 8:7737-7780. doi10.5194/amtd-8-7737-2015, 2015.

Fernald, F.G.: Analysis of atmospheric lidar observations, some commnets, Applied Optics, vol. 32, pp. 652-653, 1984.

https://doi.org/10.5194/acp-2019-565
Preprint. Discussion started: 15 July 2019

Atmospheric Chemistry and Physics Discussions

Filioglou, M., Nikandrova, A., Niemelä, S., Baars, H., Mielonen, T., Leskinen, A., Brus, D., Romakkaniemi, S., Giannakaki, E., and Komppula, M.: Profiling water vapor mixing ratios in Finland by means of a Raman lidar, a satellite and a model, Atmos. Meas. Tech., 10, 4303-4316, https://doi.org/10.5194/amt-10-4303-2017, 2017.

Freudenthaler, V., Esselborn, M., Wiegner, M., Heese, B., Tesche, M., Ansmann, A., Muller, D., Althausen, D., Wirth, M., Andreas, F. I. X., Ehret, G., Knippertz, P., Toledano, C., Gasteiger, J., Garhammer, M., and Seefeldner, M.: Depolarization ratio profiling at several wavelengths in pure saharan dust during SAMUM 2006, Tellus B, 61, 165–179, 2009.

Garnier, A., Pelon, J., Vaughan, M. A., Winker, D. M., Trepte, C.R., and Dubuisson, P.: Lidar multiple scattering factors inferred from CALIPSO lidar and IIR retrievals of semi-transparent cirrus cloud optical depths over oceans, Atmos. Meas. Tech., 8, 2759–2774, doi:10.5194/amt-8-2759-2015, 2015.

Giannakaki, E., van Zyl, P. G., Müller, D., Balis, D., and Komppula, M.: Optical and microphysical characterization of aerosol layers over South Africa by means of multi-wavelength depolarization and Raman lidar measurements, Atmos. Chem. Phys., 16, 8109-8123, https://doi.org/10.5194/acp-16-8109-2016, 2016.

Giannakaki, E., Balis, D. S., Amiridis, V., and Kazadzis, S.: Optical and geometrical characteristics of cirrus clouds over a Southern European lidar station, Atmos. Chem. Phys., 7, 5519–5530, doi:10.5194/acp-7-5519-2007, 2007.

Georgousis G., Adam M., and Avdikos G.,: Signal to noise ratio estimations for a volcanic ash detection lidar. Case Study: Met Office, 27 th International Laser Radar Conference: 5-10 July, New York, USA, 2015.

Gouveia Diego A., Barja B., Barbosa H. M. J., Seifert P., Baars H., Pauliquevis T., and Artaxo P.: Optical and geometrical properties of cirrus clouds in Amazonia derived from 1 year of ground-based lidar measurements, Atmos. Chem. Phys., 17, 3619–3636, www.atmos-chem-phys.net/17/3619/2017/, doi:10.5194/acp-17-3619-2017, 2017.

He, Q. S., and Coauthors: The properties and formation of cirrus clouds over the Tibetan Plateau based on summertime lidar measurements. J. Atmos. Sci., 70, 901–915, doi:https://doi.org/10.1175/JAS-D-12-0171.1, 2013.

Hoareau, Christophe & Keckhut, Philippe & Noel, Vincent & Chepfer, H & Baray, J.: A decadal cirrus clouds climatology from ground-based and spaceborne lidars above the south of France (43.9°N–5.7°E). Atmospheric Chemistry and Physics. 13. 10.5194/acp-13-6951-2013, 2013.

Hogan, R. J. and Kew, S. F.: A 3D stochastic cloud model for investigating the radiative properties of inhomogeneous cirrus clouds, Q. J. Roy. Meteor. Soc., 131, 2585–2608, 2005. Hogan, R. J.: "Fast approximate calculation of multiply scattered lidar returns," Appl. Opt. 45, 5984-5992, 2006.

Hong, G., Yang, P., Heidinger, A. K., Pavolonis, M. J., Baum, B. A., and Platnick, S. E: Detecting opaque and nonopaque tropical upper tropospheric ice clouds: A trispectral technique based on the MODIS 8-12 μm window bands, J. Geophys. Res., 115, D20214, doi:10.1029/2010JD014004, 2010.

Illingworth, A. J., R. J. Hogan, E. J. O'Connor, D. Bouniol, M. E. Brooks, J. Delanoe, D. P. Donovan, J. D. Eastment, N. Gaussiat, J. W. F. Goddard, M. Haeffelin, H. Klein Baltink, O. A. Krasnov, J. Pelon, J.-M. Piriou, A. Protat, H. W. J. Russchenberg, A. Seifert, A. M. Tompkins, G.-J. van Zadelhoff, F. Vinit, U. Willen, D. R. Wilson and C. L. Wrench:835 Cloudnet - continuous evaluation of cloud profiles in seven operational models using ground-based observations , Bull. Am. Meteorol. Soc., 88, 883-898, 2007.

Josset, D., Pelon, J., Garnier, A., Hu, Y., Vaughan, M., Zhai, P.-W., Kuehn, R., and Lucker, P.: Cirrus optical depth and lidar ratio retrieval from combined CALIPSO-CloudSat observations using ocean surface echo, J. Geophys. Res., 117, D05207,doi:10.1029/2011JD016959, 2012.

https://doi.org/10.5194/acp-2019-565
Preprint. Discussion started: 15 July 2019

Atmospheric Chemistry and Physics Discussions

Jylhä, Kirsti & Tuomenvirta, Heikki & Ruosteenoja, Kimmo: Climate Change projections for Finland during the 21st century. Boreal Environment Research. 9, 2004.

Kienast-Sjögren, E., Rolf, C., Seifert, P., Krieger, U. K., Luo, B. P., Krämer, M., and Peter, T.: Climatological and radiative properties of midlatitude cirrus clouds derived by automatic evaluation of lidar measurements, Atmos. Chem. Phys., 16, 7605-7621, https://doi.org/10.5194/acp-16-7605-2016, 2016.

Klett, J. D.: Stable analytical inversion solution for processing lidar returns, Appl. Opt., 20, 211–220, https://doi.org/10.1364/AO.20.000211, 1981.

Kulmala, M., Asmi, A.,Lappalainen, H.K., et al.: General overview: European Integrated project on Aerosol Cloud Climate and Air Quality interaction (EUCAARI) – integrating aerosol research from nano to global scales: Atmos. Chem. Phys., 11, 13061-13143, doi:10.5194/acp-11-13061-2011, 2011.

Komppula, M., Mielonen, T., Arola, A., Korhonen, K., Lihavainen, H., Hyvärinen, A.-P., Baars, H., Engelmann, R., Althausen, D., Ansmann, A., Müller, D., Panwar, T. S., Hooda, R. K., Sharma, V. P., Kerminen, V.-M., Lehtinen, K. E. J., and Viisanen, Y.: Technical Note: One year of Raman-lidar measurements in Gual Pahari EUCAARI site close to New Delhi in India – Seasonal characteristics of the aerosol vertical structure, Atmos. Chem. Phys., 12, 4513-4524, https://doi.org/10.5194/acp-12-4513-2012, 2012.

Laakso, L., Vakkari, V., Virkkula, A., Laakso, H., Backman, J., Kulmala, M., Beukes, J. P., van Zyl, P. G., Tiitta, P., Josipovic, M., Pienaar, J. J., Chiloane, K., Gilardoni, S., Vignati, E., Wiedensohler, A., Tuch, T., Birmili, W., Piketh, S., Collett, K., Fourie, G. D., Komppula, M., Lihavainen, H., de Leeuw, G., and Kerminen, V.-M.: South African EUCAARI measurements: seasonal variation of trace gases and aerosol optical properties, Atmos. Chem. Phys., 12, 1847-1864, https://doi.org/10.5194/acp-12-1847-2012, 2012.

Lakkis S. Gabriela, Lavorato Mario, Canziani Pablo, Lacomi Hector, Lidar observations of cirrus clouds in Buenos Aires, Journal of Atmospheric and Solar-Terrestrial Physics, Volumes 130–131, Pages 89-95, ISSN 1364-6826, https://doi.org/10.1016/j.jastp.2015.05.020. (http://www.sciencedirect.com/science/article/pii/S1364682615001194), 2015.

Liou, K. N.: Influence of cirrus clouds on weather and climate processes: A global perspective, Mon. Weather Rev., 114, 1167–1199, 1986.

Liu, J. J., Z. Q. Li, Y. F. Zheng, and M. Cribb: Cloud-base distribution and cirrus properties based on micropulse lidar measurements at a site in southeastern China. Adv. Atmos. Sci., 32(7), 991–1004, doi: 10.1007/s00376-014-4176-2, 2015.

Lynch D. K., Sassen K., Starr D.O'C. , and Stephens G.,: Cirrus, ISBN: 9780195130720.

Martins, E., Noel V., and Chepfer H., Properties of cirrus and subvisible cirrus from nighttime Cloud-Aerosol Lidar with Orthogonal Polarization (CALIOP), related to atmospheric dynamics and water vapor, J. Geophys. Res., 116, D02208, doi:10.1029/2010JD014519, 2011.

Min, M., P. Wang, J. R. Campbell, X. Zong, and J. Xia: Cirrus cloud macrophysical and optical properties over north China from CALIOP measurements. Adv. Atmos. Sci., 28(3), 653–664, doi: 10.1007/s00376-010-0049-5, 2011.

Pandit, A. K., Gadhavi, H. S., Venkat Ratnam, M., Raghunath, K., Rao, S. V. B., and Jayaraman, A.: Long-term trend analysis and climatology of tropical cirrus clouds using 16 years of lidar data set over Southern India, Atmos. Chem. Phys., 15, 13833-13848, https://doi.org/10.5194/acp-15-13833-2015, 2015.

Platt, C. M. R.: Remote sounding of high clouds. III: Monte Carlo calculations of multiple scattered lidar returns, J. Atmos. Sci., 38, 156–167, 1981.

Reichardt, J.,: Optical and geometrical properties of northern midlatitude cirrus clouds observed with a UV Raman lidar. Phys. Chem. Earth, Part B, 24, 255–260, 1999.

https://doi.org/10.5194/acp-2019-565
Preprint. Discussion started: 15 July 2019

Ross, K. E., Piketh, S. J., Bruintjes, R. T., Burger, R. P., Swap, R. J., and Annegarn, H. J.: Spatial and seasonal variations in CCN distribution and the aerosol-CCN relationship over southern Africa, J. Geophys. Res., 108, 8481, doi:10.1029/2002JD002384, 2003.

Sassen, K. and S. Benson, 2001: A Midlatitude Cirrus Cloud Climatology from the Facility for Atmospheric Remote Sensing. Part II: Microphysical Properties Derived from Lidar Depolarization. J. Atmos. Sci., 58, 2103–2112, https://doi.org/10.1175/1520-0469(2001)058<2103:AMCCCF>2.0.CO;2, 2001.

Sassen, K. and Cho, B. S.: Subvisual-Thin cirrus lidar dataset for satellite verification and climatological research, J. Appl. Meteorol., 31, 1275–1285, doi:10.1175/1520-0450(1992) 031<1275:STCLDF>2.0.CO 2 , 1992.

Sassen, K., Z. Wang, and D. Liu, Global distribution of cirrus clouds from CloudSat/Cloud-Aerosol Lidar and Infrared Pathfinder Satellite Observations (CALIPSO) measurements, J. Geophys. Res., 113, D00A12, doi:10.1029/2008JD009972, 2008.

Seifert, P., Ansmann, A., Muller, D., Wandinger, U., Althausen, D., Heymsfield, A. J., Massie, S. T., and Schmitt C.: Cirrus optical properties observed with lidar, radiosonde, and satellite over the tropical Indian Ocean during the aerosol-polluted northeast and clean maritime southwest monsoon, J. Geophys. Res., 112, D17205, doi:10.1029/2006JD008352, 2007.

Wandinger, U.: Multiple-scattering influuence on extinction- and backscatter-coefficient measurements with Raman and high-spectral resolution lidars, Appl. Opt., 37, 417–427, 1998.

Young, S. A. and Vaughan, M. A.: The Retrieval of Profiles of Particulate Extinction from Cloud-Aerosol Lidar Infrared Pathfinder Satellite Observations (CALIPSO) Data: Algorithm Description, J. Atmospheric Ocean. Technol., 26, 1105–1119,doi:10.1175/2008JTECHA1221.1, 2009.

Young, S. A., Vaughan, M. A., Kuehn, R. E., and Winker, D. M.: The Retrieval of Profiles of Particulate Extinction from Cloud–Aerosol Lidar and Infrared Pathfinder Satellite Observations (CALIPSO) Data: Uncertainty and Error Sensitivity Analyses, J. Atmospheric Ocean. Technol., 30, 395–428, doi:10.1175/JTECH-D-12-00046.1, 2013.

https://doi.org/10.5194/acp-2019-565
Preprint. Discussion started: 15 July 2019

Atmospheric Chemistry and Physics Discussions

Table 1. Technical specifications of the Polly^{XT} System.

Characteristics	Polly^{XT}
Operating Wavelength(s)	355nm, 532nm, 1064nm
Average pulse energy	∼450 mJ
Laser beam divergence	<0.2 mrad
Telescope diameter	0.3m
Receiver field of view	1mrad
Detectors	Hamamatsu PMTs
Polarization	Cross & Total
Raw data range resolution	30m
Raw data time resolution	30s

https://doi.org/10.5194/acp-2019-565
Preprint. Discussion started: 15 July 2019

Atmospheric Chemistry and Physics Discussions

Table 2. Number of detected cirrus layers, percentages of each cirrus category, mean values of Lidar Ratio and the particle depolarization for the three regions.

Station	N	% subvisible	% thin	% opaque	LR 355	LR 532	Particle depol
Kuopio	229	3	70	27	33 ± 7	30 ± 8	0.38
Gual Pahari	25	0	28	72	26 ± 12	27 ± 16	-
Elandsfontein	88	4	52	44	25 ± 6	24 ± 6	-

https://doi.org/10.5194/acp-2019-565
Preprint. Discussion started: 15 July 2019

Atmospheric Chemistry and Physics Discussions

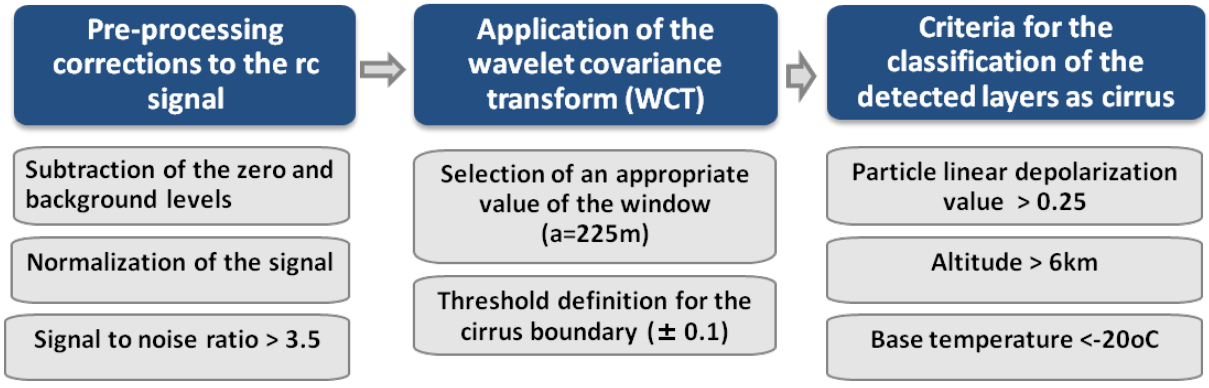

Figure 1. Schematic flowchart showing the main steps of the methodology applied in this study to obtain the cirrus geometrical boundaries from the Polly^{XT} measurements.

https://doi.org/10.5194/acp-2019-565
Preprint. Discussion started: 15 July 2019

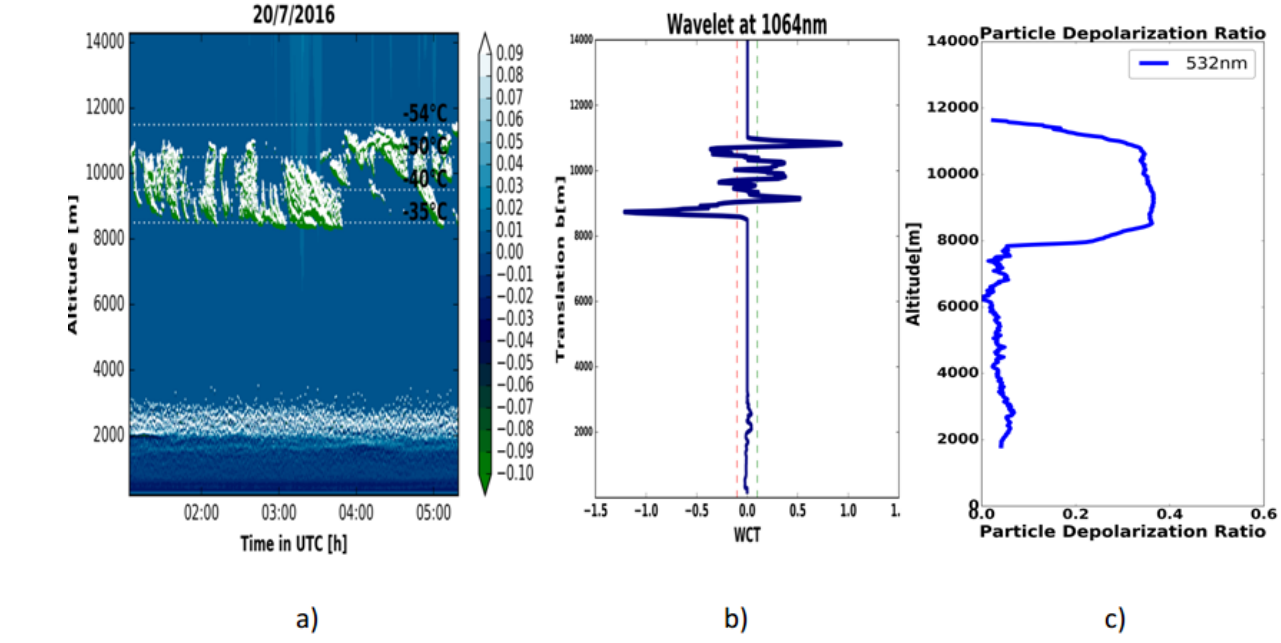

Figure 2. Cirrus cloud evolution as determined from the Polly^{XT} observations (a), the averaged wavelet applied to the corrected 1064 signal (b) and the mean particle Depolarization ratio for the whole period of study (c) on 20th of July 2016 at Kuopio station.

https://doi.org/10.5194/acp-2019-565
Preprint. Discussion started: 15 July 2019

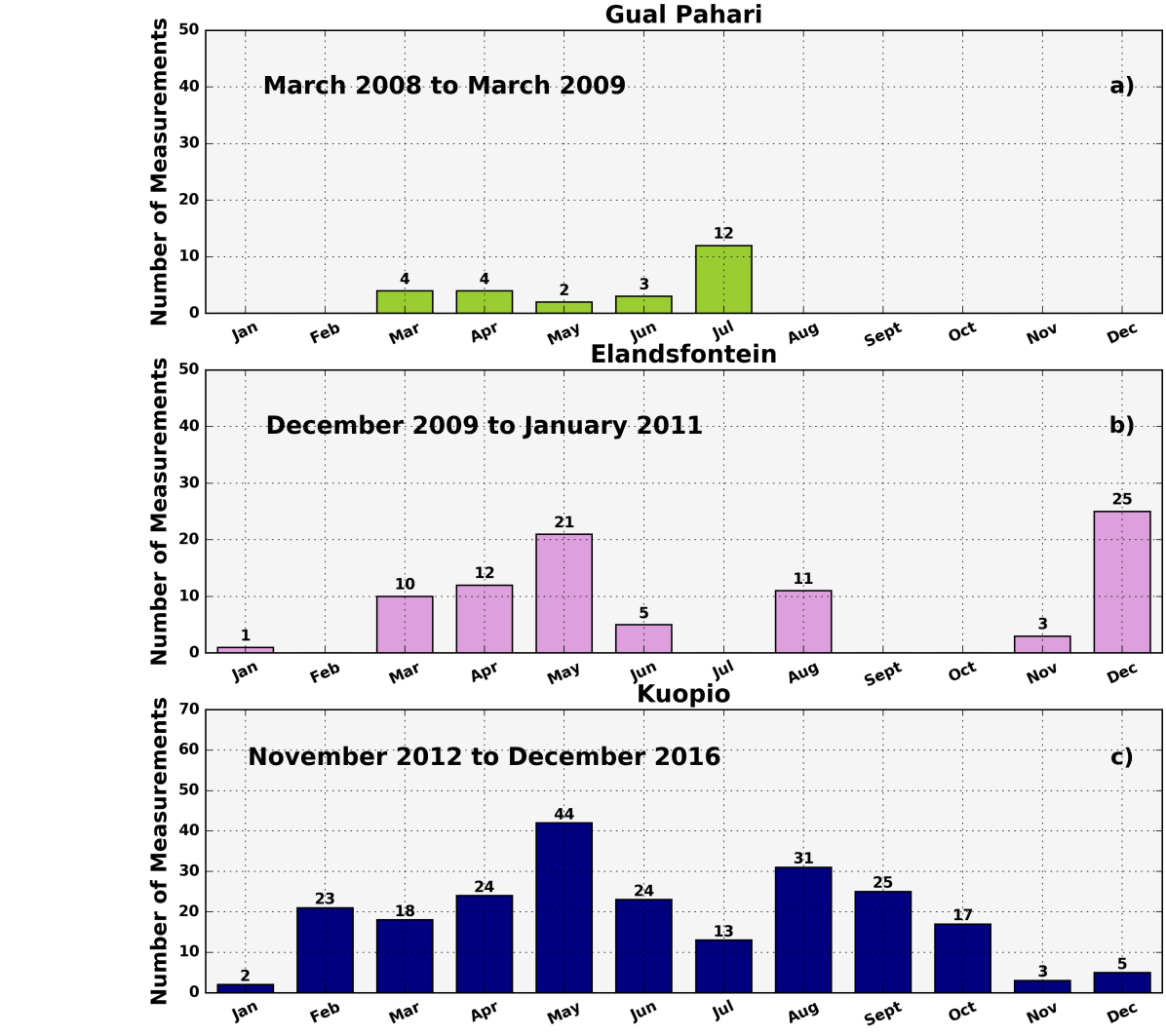

Figure 3. Cirrus detection with the Polly^{XT} over Gual Pahari, India during the period 2008-2009 (a) Elandsfontein, South Africa during the period 2009-2010(b) and Kuopio (c), Finland during 2014-2016.

https://doi.org/10.5194/acp-2019-565
Preprint. Discussion started: 15 July 2019

Atmospheric Chemistry and Physics Discussions

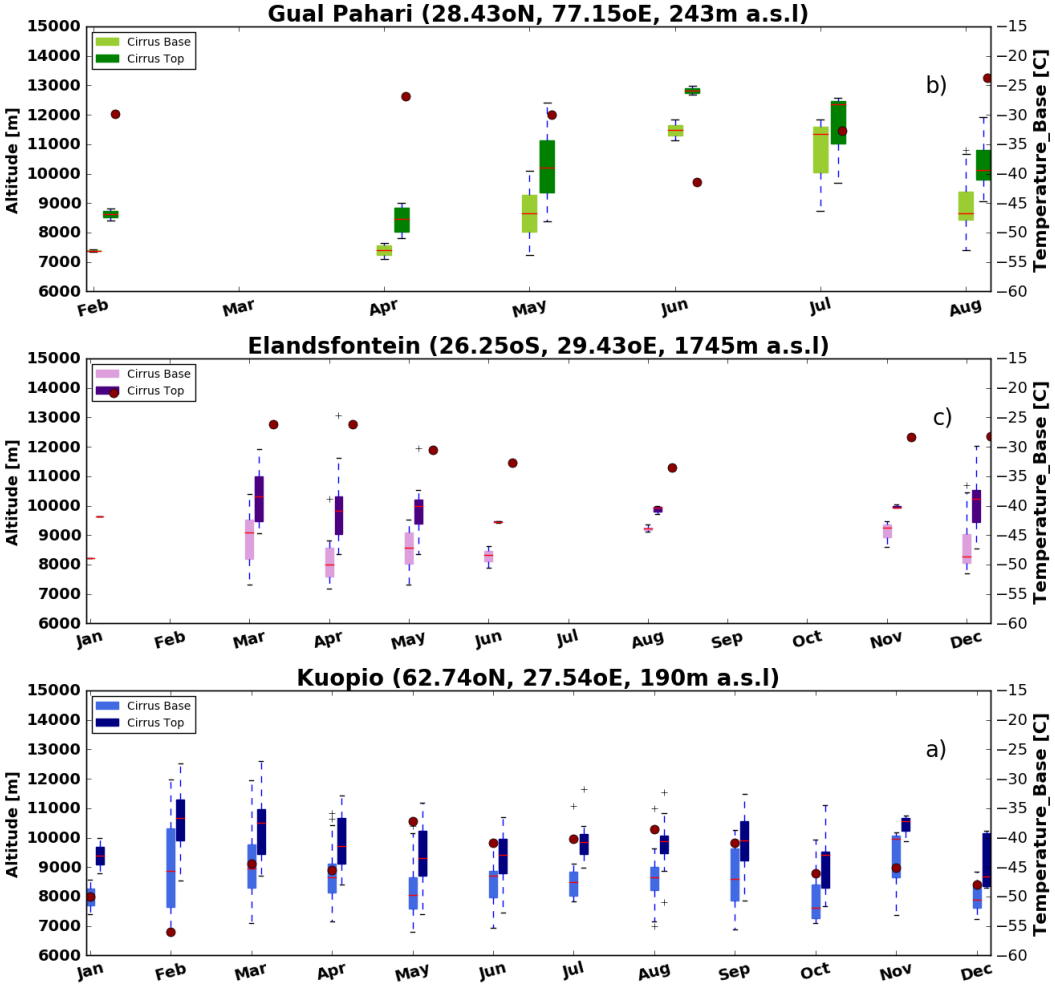

Figure 4. Monthly cycle of mean base, mean top and the corresponding temperature base values (circles) of the cirrus clouds at Kuopio (a), Gual Pahari (b) and Elandsfontein (c). Horizontal line in box: median. Boxes: the upper and lower quartile. Whisker: extreme values.

https://doi.org/10.5194/acp-2019-565
Preprint. Discussion started: 15 July 2019

Atmospheric Chemistry and Physics Discussions

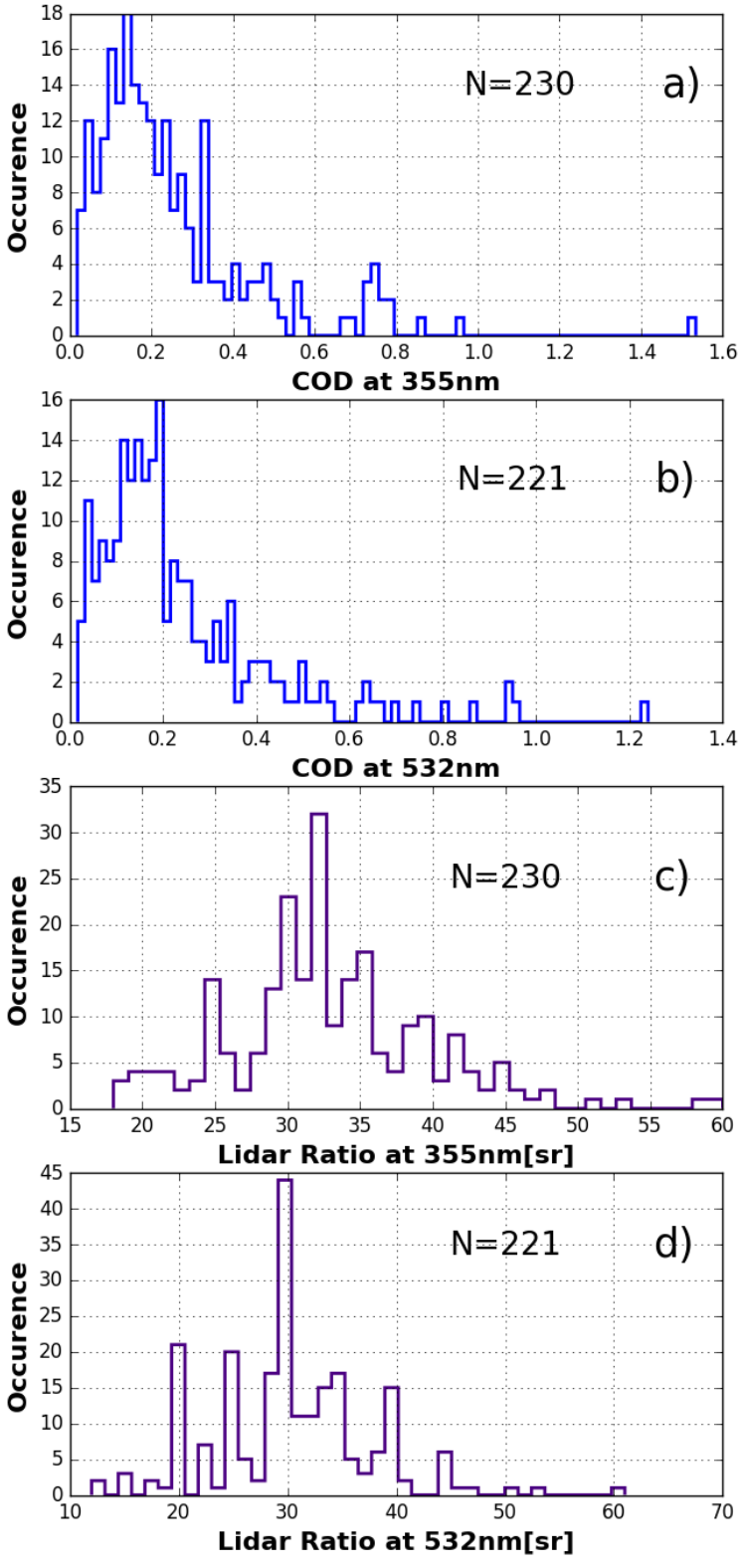

Figure 5. Histograms of (a) the COD at 355nm, (b) the COD at 532nm, (c) the Lidar Ratio at 355nm and (d) the Lidar Ratio at 532nm of the cirrus detected layers observed over Kuopio, Finland.

https://doi.org/10.5194/acp-2019-565
Preprint. Discussion started: 15 July 2019

Atmospheric Chemistry and Physics Discussions

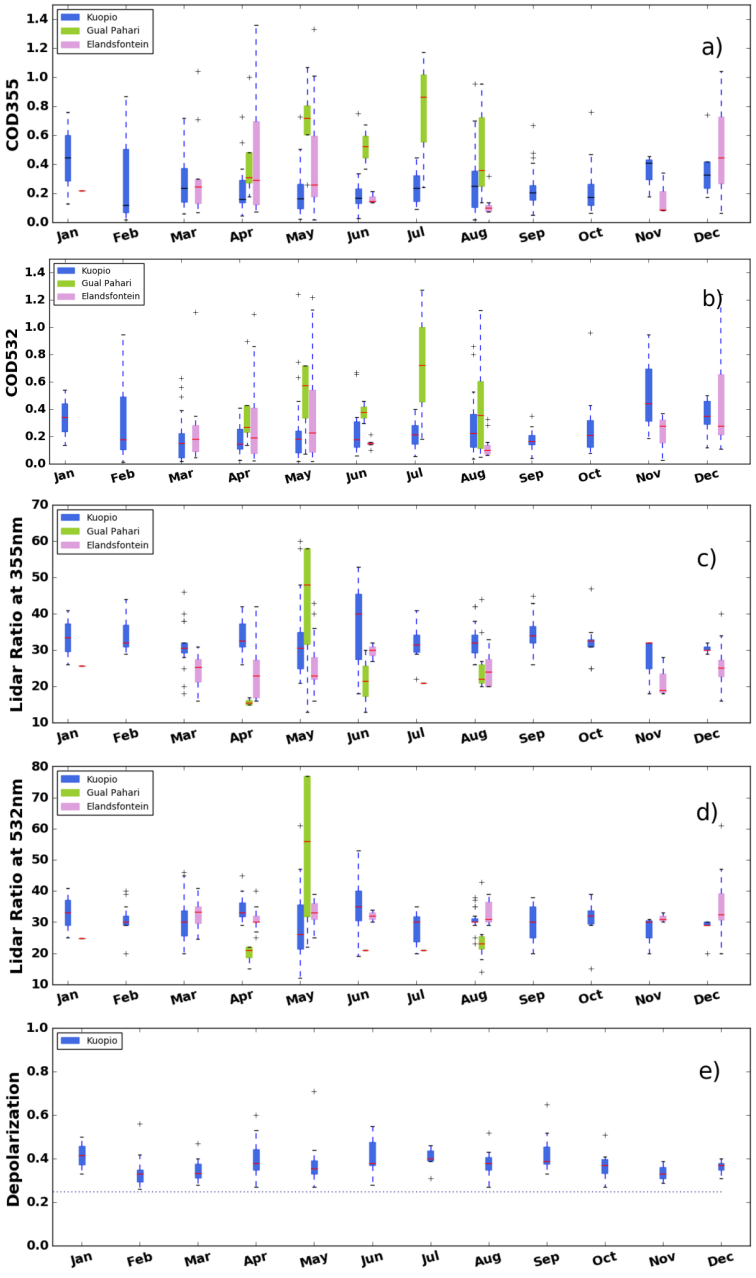

Figure 6. (a) Mean optical depth (multiple scattering corrected) values at 355nm, (b) mean optical depth (multiple scattering corrected) values at 532nm, (c) Lidar Ratio at 355nm, (d) Lidar Ratio at 532nm and (e) particle depolarization ratio for the detected cirrus layers for the study period of the three regions. Horizontal line in box: median. Boxes: the upper and lower quartile. Whisker: extreme values. Red line stands for the mean values for every month.

https://doi.org/10.5194/acp-2019-565
Preprint. Discussion started: 15 July 2019

Atmospheric Chemistry and Physics Discussions

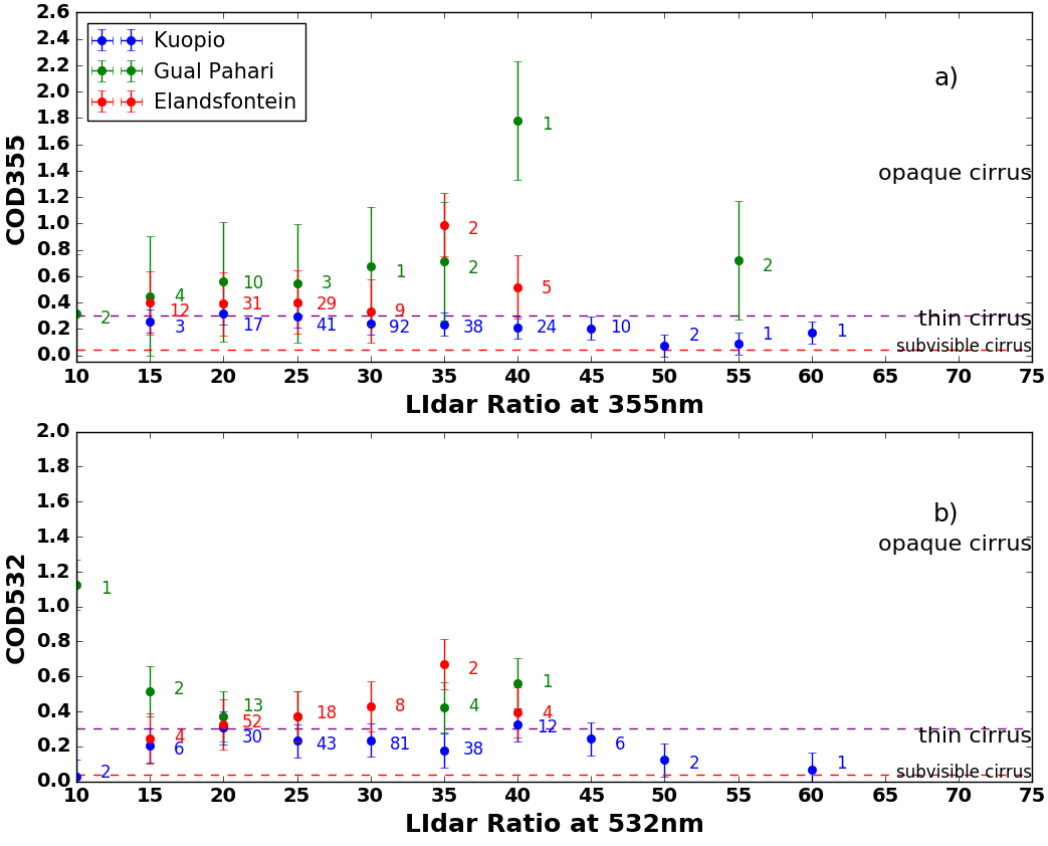

Figure 7. Dependence of (a) the corrected lidar ratio with COD at 355nm and (b) the corrected lidar ratio with COD at 532nm. Numbers labeled indicate the number of cases per lidar ratio bin. Horizontal dashed lines: cirrus categories by Sassen and Cho (1992).

https://doi.org/10.5194/acp-2019-565
Preprint. Discussion started: 15 July 2019

Atmospheric Chemistry and Physics Discussions

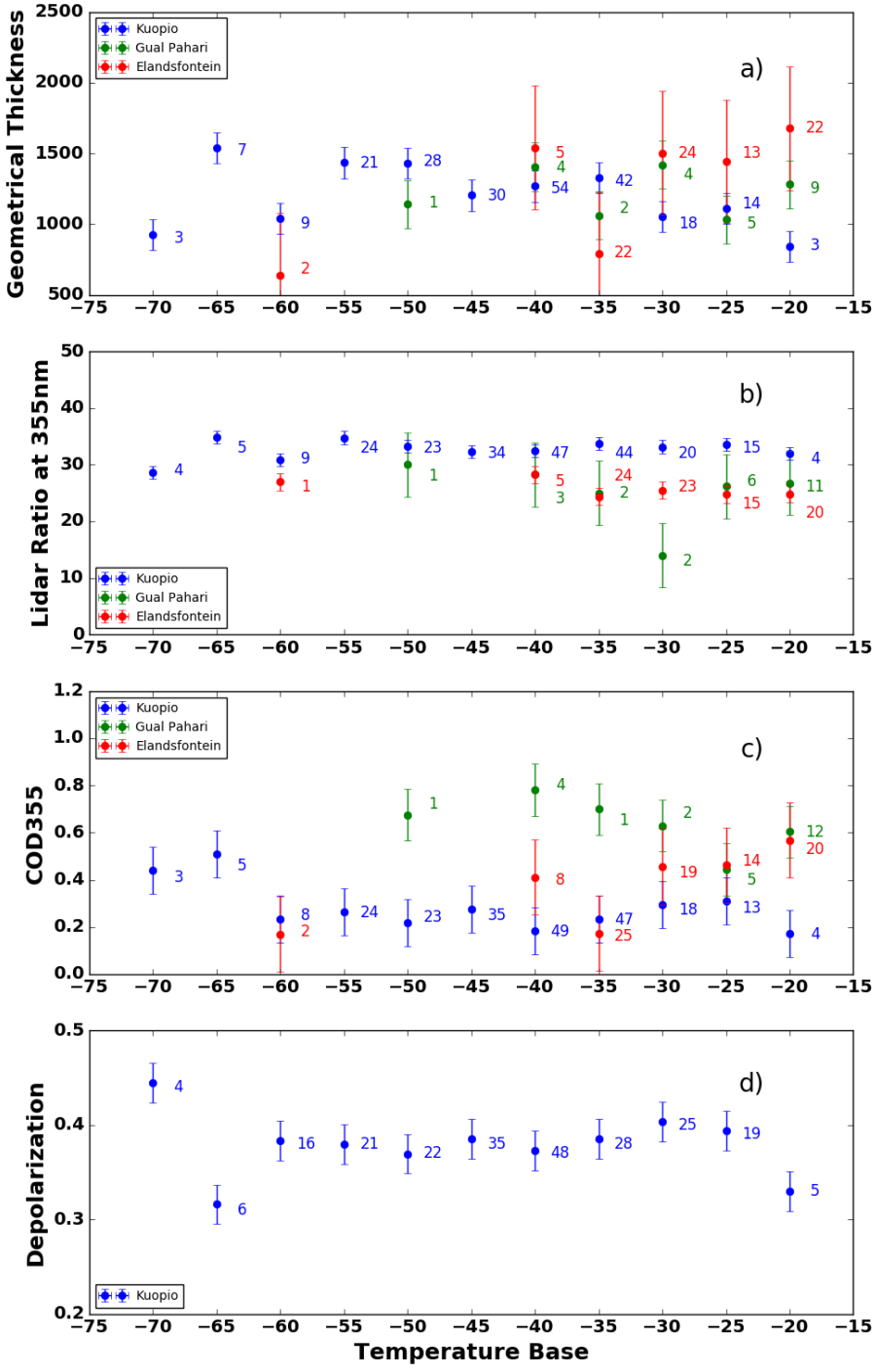

Figure 8. Dependencies of (a) geometrical thickness, (b) lidar ratio, (c) optical depth at 355nm and (d) particle depolarization values on 5°C intervals of cirrus base temperature. Numbers labeled indicate the number of cases per temperature bin.